Small hole polarons in yellow phase δ-$CsPbI_3$

Yun Liu*

*Institute of High Performance Computing (IHPC), Agency for Science, Technology and Research (A*STAR), 1 Fusionopolis Way, #16-16 Connexis, Singapore 138632, Republic of Singapore*

E-mail: liu_yun@ihpc.a-star.edu.sg

Abstract

A heterophase containing both the optically active α-$CsPbI_3$ and non-active δ-$CsPbI_3$ has been demonstrated as an efficient white light emitter. This has challenged the conventional perspective that non-active phases of perovskites are undesirable in any perovskite-based optoelectronic devices. To understand the role that the yellow phase δ-$CsPbI_3$ plays in the light emission process, we performed a systematic computational study on its electronic and optical properties, which are relatively unexplored in the literature. Using the Fröhlich model we showed that the electron and hole both exhibit moderate coupling to longitudinal optical phonons. Explicit density functional theory calculations show that small hole polarons exist with a formation energy of -96 meV, corresponding to the contraction of the Pb-I bonds within a [PbI_6] octahedra and wavefunction localization. Molecular dynamics simulations showed that the small hole polaron is stable against thermal disorder, and exhibit periodic localization and delocalization behavior similar to carrier hopping with a characteristic lifetime of 0.3 ps. Our results might have elucidated the role that δ-$CsPbI_3$ play in the self-trapped emission in perovskite-based white light emitting diodes by supporting the presence of a localized small hole polaron.

Lead halide perovskites have been widely investigated due to their desirable bandgaps, high photoluminescence quantum yields, low nonradiative rate, and solution processable synthesis.[1–4] The high optoelectronic performance of these perovskites-based devices rely on their crystal structures staying in the optically active black phases at ambient conditions. Even during normal device operations, methylammonium lead iodides ($MAPbI_3$) are prone to chemical degradation upon exposure to moisture and oxygen, leading to the formation of undesirable side products such as PbI_2.[5–8] Formamidinium (FA) and Cs-based compositions have improved chemical stability compared to their MA counterpart, but their optically active α, β or γ-phases can also quickly transform into the thermodynamically more stable nonperovskite hexagonal and orthorhombic δ-phases respectively.[9] As these δ-phases are optically inactive, they are typically detrimental to the device performances. Therefore, various strategies such as encapsulation, surface passivation and chemical alloying have been developed to improve their phase stabilities.[4,6,7,10,11]

While conventional wisdom dictates that the presence of yellow phases need to be minimized at all cost, recent evidence suggests that they might play an important role in many interesting light emission phenomena. For example, intrinsic quantum confinement with the co-existence of α- and δ-$FAPbI_3$ has manifested as oscillatory absorption spectra.[12] It was hypothesized that the δ-phases, with its larger bandgap, act as potential barriers resulting in nanostructures of α-phases with a typical length scale of $10 - 20\,\text{nm}$. The transformation into the δ-phase can also be suppressed by alloying Cs atoms, leading to the ability to control the degree of quantum confinement.[13] Light emission from these quantum confined regions can potentially be used as single-photon sources analogous to colloidal quantum dots.[14,15]

In addition, efficient and bright white light emitting diodes (LED) have been synthesized based on the heterophases of α and δ-$CsPbI_3$.[16,17] The carrier injection and transport were dominated by the optically active α-phase, with the charges ultimately injected into the δ-phase where efficient radiative recombination occurred *via* self-trapped excitons (STE). The synergetic cooperation between the two phases are hypothesized to achieve the high

efficiency and brightness observed in the white LED.[17]

Carrier self-trapping in semiconductors occurs when excited carriers and the locally distorted lattice form a quasi-particle called polaron.[18] Polarons can be classified into two types based on the strength of the electron-phonon coupling. Large polarons are formed due to the long-range interaction between electrons/holes and the longitudinal optical (LO) phonons. In halide perovskites, large polarons are known to be responsible for the long carrier diffusion lengths[19–22] and enhanced effective masses.[23] Their formation kinetics have been observed in pseudocubic $CsPbBr_3$, and first-principles calculation showed that the hole polaron can extend over 8 unit cells in one direction.[24]

Stronger coupling between charge carriers and phonons leads to larger local lattice distortions that provide the driving force for small polarons to form. The motion of small polarons have been observed in low dimensional perovskites and are characterized by incoherent phonon assisted hopping with much smaller carrier mobility.[25–28] The existence and formation mechanism of small polarons in 3D perovskites are not conclusive.[29] For δ-$CsPbI_3$, even the most basic optoelectronic properties are not understood, and it is therefore not clear what role it plays in the light emission processes in perovskite-based devices. Here in this work, we present a systematic investigation of the electronic structure of δ-$CsPbI_3$. We utilized a combination of Fröhlich polaron model, density functional theory (DFT) and *ab initio* molecular dynamics (MD) calculations to show that small hole polarons are stable in δ-$CsPbI_3$, which can potentially support carrier self-trapping and STE mediated emissions.

Results and Discussion

We first evaluated the ground state electronic and structural properties of δ-$CsPbI_3$, which belongs to the orthorhombic space group *Pmna* with 20 atoms per unit cell. Adjacent $[PbI]_6$ octahedra share a common edge (Figure 1(a)), in contrast to the corner sharing in α, β and γ-phases. The lattice parameters obtained with the PBEsol functional at $a = 10.41\,\text{Å}$ $b =$

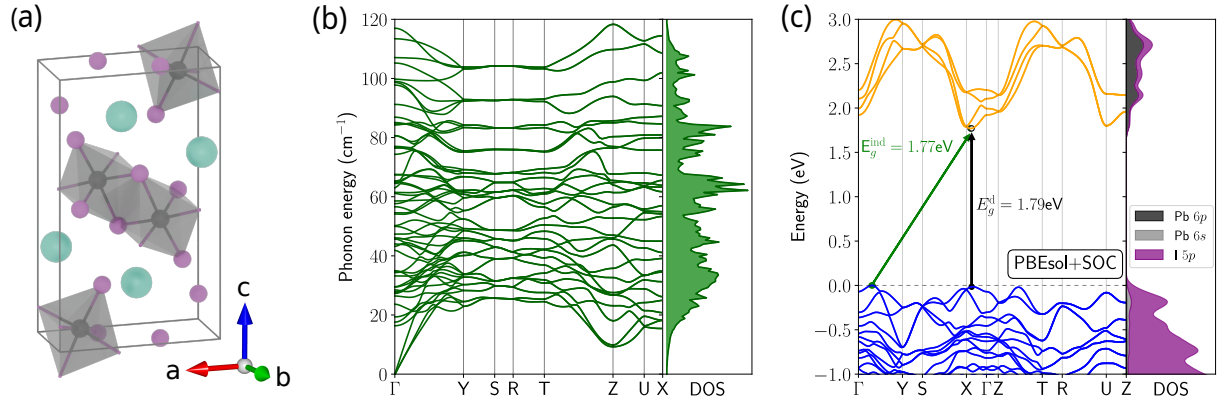

Figure 1: Ground state properties. (a) Crystal structure of δ-$CsPbI_3$ where Cs, Pb and I atoms are represented as cyan, black and purple spheres with the $[PbI]_6$ polyhedron drawn. (b) The phonon dispersion along high symmetry lines of the Brillouin zone with the total phonon density of states on the right panel. (c) Electronic band structure and projected density of states (PDOS) along high-symmetry lines at the PBEsol+SOC level, with the location of the indirect band edge locations (E_g^{ind}) indicated by green circles, and that of the direct band edge locations (E_g^{d}) indicated by black circles.

4.76 Å, and $c = 17.66$ Å agree well with the experimental values of $a = 10.45$ Å $b = 4.80$ Å, and $c = 17.76$ Å.[30] The computed phonon dispersion and phonon density of states (DOS) are shown in Figure 1(b), which exhibits no soft modes indicating dynamical stability. Figure 1(c) shows the band structure and projected DOS (PDOS) of δ-$CsPbI_3$ with the effects of spin-orbit coupling (SOC) included due to the presence of the Pb atom. The valence band maximum (VBM) consists of mainly I $5p$ orbitals and the conduction band minimum (CBM) is dominated by Pb-I bonds made up of Pb $6p$ and I $5p$ orbitals.

δ-$CsPbI_3$ is an indirect bandgap semiconductor, as the positions of the VBM and CBM are located away from Γ at (0.0, 0.15, 0.0) and (0.39, 0.0, 0.0), respectively. The indirect bandgap E_g^{ind} is 1.77 eV at the PBEsol+SOC level, while the direct bandgap $E_g^{\mathrm{d}} = 1.79$ eV is only about 20 meV higher than that of E_g^{ind}. Due to this small difference, δ-$CsPbI_3$ can be treated as an effective direct bandgap semiconductor. We note that the bandgaps are underestimated due to the well-known errors in semilocal DFT functionals.

We then estimate the strength of the electron-phonon coupling (α) using the Fröhlich model (Details in the Supplementary Information). Within this model, the electron-phonon

Table 1: The electron and hole effective masses, dimensionless Fröhlich polaron constants and Schultz polaron radii of δ-$CsPbI_3$ at 300 K.

	$m*$ (m_e)		α		r_f (Å)	
	e^-	h^+	e^-	h^+	e^-	h^+
average	0.51	0.86	3.25	4.22	21.9	19.2
x	0.65	0.82	3.68	4.12	20.6	19.4
y	0.26	0.82	2.31	4.12	26.1	19.4
z	2.11	0.96	6.61	4.46	15.2	18.7

interaction is dominated by the LO phonon modes, which gives an estimate of the potential deformation the charge carriers on the surrounding lattice. The Fröhlich polaron constants for electrons shown in Table 1 exhibit strong anisotropy. This can be explained from the highly anisotropic crystal structure of δ-$CsPbI_3$ whereby the corner sharing $[PbI]_6$ octahedra extend infinitely along the y direction giving rise to more disperse band structures. The octahedra are separate by the Cs atoms along the x and z directions, resulting in more flat bands as the Cs orbitals do not directly contribute to the band edge states.

The average values of α ($3.25-4.22$) are in the intermediate coupling regime ($3 < \alpha < 6$), larger than the typical values for the black phases ($1.17 - 2.68$[31]). The increase is mainly due to the larger effective masses in δ-$CsPbI_3$, as the characteristic phonon frequencies are similar between the different phases. The Fröhlich coupling constants of δ-$CsPbI_3$ are closer to those of 2D and double perovskites, which means that it has the potential to exhibit similar spectroscopic signatures such as broadband emission arising from strong carrier self-trapping.[31] We then estimated the Schultz polaron radius (r_f) at 300 K which also exhibits strong anisotropy. Along the z direction, r_f is comparable to the c unit cell lattice parameter, whereas along x and y directions, r_f spans over multiple unit cells.

We want to highlight the importance of dimensionality for localized carrier formation. In 3D and 2D systems, the local lattice deformations arising from the strong coupling between carrier and phonons generate a potential barrier acting as a trap, and free carriers need to overcome this barrier to self-trap.[32–34] In 1D, the barrier is effectively zero, and free and excited carriers can co-exist. While δ-$CsPbI_3$ is structurally a 3D system, the strong

anisotropy in its electronic structures show that its electronic dimensionality is closer to that of a pseudo-1D system, as the the bonding orbitals arising from the [PbI_6] octahedra form 1D chains along the y directions.[35] The pseudo-1D electronic structure might favor easier formation of the self-trapped carriers in δ-$CsPbI_3$ compared to its black phase counterpart.

As the Fröhlich model treats the electron phonon interaction as a low order perturbation in a harmonic lattice potential, it has its limitations to fully describe the polaronic behavior in perovskites due to their soft anharmonic lattice.[36] For an alternative assessment, we performed direct first-principles DFT calculations. Hybrid functionals are used to accurately describe wavefunction localization associated with polarons[37–39] and to minimize the self-interaction errors commonly associated with semilocal functionals.

For accurate descriptions of polaron properties with hybrid functionals, we first need to determine the fraction of exact Fock exchange that fulfills the Koopmans' conditions.[40] To do so we calculated the occupied and unoccupied single particle energy levels related to transition of unrelaxed iodine and lead vacancies, by varying the amount of Fock exchange in unscreened PBE0 hybrid functional.[41,42] Figure S1 shows the computed band edges and the energy levels for the V_I(+/0) and V_{Pb}(-1/-2) transitions including the effects of SOC and finite-size corrections.[43–45] The crossing between the different charge states of the same defect corresponds to the value of exact exchange for which the Koopmans' condition is satisfied. For both defects, this crossing occurs at 0.12. We note that this value is substantially lower than the value of 0.28 obtained for α-$CsPbI_3$.[46] This might be due to the lower defect tolerance of δ-$CsPbI_3$ which contains a larger octahedral tilt associated with the smaller Pb-I-Pb bond lengths and the weak anitbonding characteristic of the CBM state.[47] This further illustrates that the different polymorphs of $CsPbI_3$, especially between the perovskite and nonperovskite phases, exhibit large differences in their electronic structures. At the Fock exchange value of 0.12, the bandgap is 2.67 eV, which is in better agreement with the experimentally measured value of 2.93 eV,[48] and much improved compared to the bandgap obtained earlier from the semilocal PBEsol functional.

We then applied the bond distortion method[49–51] to various bonds in δ-$CsPbI_3$ to break the crystal structure symmetries. The atomic positions within the supercell are then relaxed in the presence of an excess electron or hole to obtain the geometry of the localized polaron structure. With an excess electron, the distorted structures always return to the ground state equilibrium after relaxation(Fig. 2[a][b]), with the wavefunction of the CBM state closely resembling that of the ground state(Fig. S2[a][b]). This shows that small electron polarons in δ-$CsPbI_3$ are unlikely to form. For the excess hole, there is significant wavefunction localization around a single [PbI_6] octahedron(Fig. 2(c)(d)), accompanied by the contraction of the Pb-I bonds by around 0.1 Å(Fig. 2(e)). There is a smaller degree of wavefunction localizing on the nearby edge sharing [PbI_6] octahedron. The hole polaron state appears just above the VBM (Fig. 2(f)) with a formation energy of -96 meV. Our DFT calculation shows that small hole polaron might be stable in δ-$CsPbI_3$, and illustrates the limitation of the Fröhlich model at characterizing systems with small polarons.

To further assess the possible presence of localized holes and electrons in the form of STE, we performed MD simulations of the system in a spin triplet configuration. The electrons are fixed using a constrained DFT approach (Details in Methods section), and the spin triplet configuration is typically more stable than the spin singlet state.[52] The system was initiated using the distorted geometry of the hole polaron, and the degree of the electron and hole wavefunction localization was quantified using the Inverse Participation Ratio (IPR)

$$\mathrm{IPR} = \frac{\sum_i |\Phi_i|^4}{(\sum_i |\Phi_i|^2)^2} \tag{1}$$

where Φ_i is the electronic wavefunction. In this definition of IPR, a localized state has a value of 1. For complete delocalization, the IPR tends towards $\frac{1}{V} = 3.25 \times 10^{-6}$ where V is the volume or the total number of grid points used to sample the system.

Fig. 3(a) shows that for the duration of the MD simulation, the electron stays delocalized with the IPR value mostly staying below 1.0×10^{-5}. On the other hand, the hole undergoes

cycles of localization and delocalization corresponding to a hopping motion with a period of 0.3 ps between 0.6 and 1.2 ps. Fig. 3(b)(c)(d) show the snapshot of the hole polaron localized in different part of the supercell at 0.6, 0.9 and 1.2 ps, respectively. The hole and electron generally gets more delocalized over time, but the hole polaron seems to be stable against thermal disorder by maintaining a significant IPR value for the duration of the MD run. Overall, the MD results further support the static DFT calculations to show that small hole polarons can form in δ-$CsPbI_3$, while small electron polaron is unlikely to form. While the constrained DFT do take into account some amount of exchange interaction between the electrons and holes, advances in accurate evaluation of excited state forces are needed to fully account for the excitonic interaction between them.

Conclusion

In conclusion, we systematically investigated the existence of polarons and STE in δ-$CsPbI_3$. The Fröhlich model predicts moderate coupling between the LO phonons and charge carriers with Fröhlich polaron constants of around $3.25 - 4.22$ and Schultz radii of ~ 20 Åat 300 K. The stronger coupling and high anisotropy in its electronic structure favor the formation of small polarons in δ-$CsPbI_3$. Explicit DFT calculations using hybrid functionals and advanced structure searching methods show that small hole polaron is stable with a formation energy of -96 meV. MD runs with the electron and holes in a triplet spin configuration show that the hole polaron is stable against thermal disorder at 300 K, and exhibit characteristic hopping with a period of 0.3 ps. Our results might have elucidated the role that δ-$CsPbI_3$ play in the self-trapped emission in perovskite-based white light emitting diodes by supporting the presence of a localized small hole polaron. There are some reports suggesting that electron polaron might be stable in α-$CsPbI_3$ clusters,[53] highlighting the possibility that STE might exist in the heterophases of δ-$CsPbI_3$ and α-$CsPbI_3$, with the electron polaron and hole polaron localized onto the different perovskite phases. To fully understand the nature of

self-trapped emission in perovskite based white LEDs, a systematic study of the crystal and electronic structure of the heterophases is needed.

Methods

Ground state electronic structure, phonon and polaron calculations were performed using the Vienna Ab initio Simulation Package (VASP, v6.4).[54,55] The core-valence interaction was described using the projector-augmented wave (PAW) method,[56] with 9 valence electrons for Cs ($5s^2 5p^6 6s^1$), 14 valence electrons for Pb ($5d^{10} 6s^2 6p^2$), and 7 valence electrons for I ($5s^2 5p^5$). The electronic wavefunctions were expanded in a plane wave basis with a cutoff of 400 eV. For structural relaxations, atoms were relaxed until the Hellman-Feynman force converges below 10^{-3} eVÅ^{-1}, and the volume until all components of the stress tensor are below 10^{-2} GPa. The Brillouin zone of the unit cell was sampled with a $4 \times 8 \times 2$ Γ-centered Monkhorst-Pack[57] **k**-point grid. The band structure and projected density of states were computed using the PBEsol functional,[58] and spin-orbit coupling (SOC) effects are included due to the presence of heavy Pb atoms. The Fröhlich polaron properties were solved using the package PolaronMobility,[59] with the input parameters obtained from ASMET.[60]

The phonon dispersion was computed using the finite displacement method with a $2 \times 4 \times 1$ supercell containing 160 atoms with a $2 \times 2 \times 2$ **k**-point grid as implemented in the Phonopy package.[61] A non-analytical term was added to the dynamical matrix to treat the long range interaction arising from the macroscopic electric field induced by the polarization of collective ionic motions near Γ.[62]

For polaron and defects calculations, we used a $2 \times 4 \times 1$ supercell to minimize spurious interactions between periodic images, and sampled only the Γ-point. For the fulfillment of the Koopmans' condition, the corrections to the unoccupied Kohn-Sham eigenvalues of the

defect-induced single particle levels were calculated as[63]

$$\epsilon_{\text{corr}}^{\text{KS}} = \frac{-2}{q} E_{\text{corr}} \tag{2}$$

where q is the charge of the defect, and E_{corr} is finite-size electrostatic correction. E_{corr} is computed using SXDEFECTALIGN,[43] where the diagonal terms of the static dielectric tensor (ε_∞) are used for anisotropic screening.

After the addition or removal of an electron, structural relaxations were performed using spin-polarized calculations whereby the supercell lattice parameters are fixed and the atoms allowed to move, with the same force convergence criterion of $10^{-3}\,\text{eV}\,\text{Å}^{-1}$. The binding energy of the hole polaron can be estimated by modifying the defect formation energy formula:[64]

$$E_b = E_q[\text{polaron}] - E[\text{pristine}] + qE_{\text{VBM}} + E_{\text{corr}} \tag{3}$$

where E_q[polaron] is the total energy of the distorted supercell of the hole polaronic state, E[pristine] is the total energy for the perfect crystal using an equivalent supercell, with q denoting the excess of charge of a hole ($q = +1$), E_{VBM} is the position of the VBM. The diagonal components of the total dielectric tensor (ε_0) were used.

The MD simulation was carried out in the NVT ensemble in a 160-atom supercell within CP2K[65,66] code, with the lattice parameters set to the equilibrium volume obtained with hybrid functional (PBE0 with 0.12 Fock exchange). To model the self-trapped exciton (STE), the constrained DFT (cDFT) or ΔSCF method was used to promote an electron from the VBM to the CBM in a spin triplet configurations with unrestricted spin-polarization. We used DZVP-MOLOPT basis sets[67,68] and the plane wave cutoff energy of 400 Ry and core-valence interactions were described by Goedecker-Teter-Hutter pseudopotentials.[69] The simulation was performed with the auxiliary density matrix method (ADMM).[70] The temperature was set to 300 K and controlled by a Nosé-Hoover thermostat[71,72] with a time step of

1 fs.

Crystal structures and isosurfaces are visualized using BLENDER[73] and BEAUTIFUL ATOMS.[74]

Acknowledgement

Y.L acknowledges funding support from A*STAR under its Young Achiever Award and Career Development Fund (C233312001). This work is supported by A*STAR Computational Resource Centre (ACRC) and National Supercomputing Centre (NSCC), Singapore, through use of their high-performance computing facilities.

Supporting Information Available

The data that support the plots within this paper and other findings of this study are available at the following Online Repository: https://doi.org/XXXXX.

References

(1) Stranks, S. D.; Snaith, H. J. Metal-halide perovskites for photovoltaic and light-emitting devices. *Nature Nanotech* **2015**, *10*, 391–402.

(2) Jena, A. K.; Kulkarni, A.; Miyasaka, T. Halide Perovskite Photovoltaics: Background, Status, and Future Prospects. *Chemical Reviews* **2019**, *119*, 3036–3103.

(3) Liu, X. K.; Xu, W.; Bai, S.; Jin, Y.; Wang, J.; Friend, R. H.; Gao, F. Metal halide perovskites for light-emitting diodes. *Nature Materials* **2020**, *20*, 10–21.

(4) Yoo, J. J.; Seo, G.; Chua, M. R.; Park, T. G.; Lu, Y.; Rotermund, F.; Kim, Y. K.; Moon, C. S.; Jeon, N. J.; Correa-Baena, J. P.; Bulović, V.; Shin, S. S.; Bawendi, M. G.;

Seo, J. Efficient perovskite solar cells via improved carrier management. *Nature* **2021**, *590*, 587–593.

(5) Dunfield, S. P.; Bliss, L.; Zhang, F.; Luther, J. M.; Zhu, K.; van Hest, M. F. A. M.; Reese, M. O.; Berry, J. J. From Defects to Degradation: A Mechanistic Understanding of Degradation in Perovskite Solar Cell Devices and Modules. *Advanced Energy Materials* **2020**, *10*, 1904054.

(6) Boyd, C. C.; Cheacharoen, R.; Leijtens, T.; McGehee, M. D. Understanding Degradation Mechanisms and Improving Stability of Perovskite Photovoltaics. *Chemical Reviews* **2019**, *119*, 3418–3451.

(7) Domanski, K.; Alharbi, E. A.; Hagfeldt, A.; Grätzel, M.; Tress, W. Systematic investigation of the impact of operation conditions on the degradation behaviour of perovskite solar cells. *Nat Energy* **2018**, *3*, 61–67.

(8) Mosconi, E.; Azpiroz, J. M.; De Angelis, F. *Ab Initio* Molecular Dynamics Simulations of Methylammonium Lead Iodide Perovskite Degradation by Water. *Chem. Mater.* **2015**, *27*, 4885–4892.

(9) Masi, S.; Gualdron-Reyes, A. F.; Mora-Sero, I. Stabilization of Black Perovskite Phase in $FAPbI_3$ and $CsPbI_3$. *ACS Energy Letters* **2020**, *5*, 1974–1985.

(10) Ding, X.; Cai, M.; Liu, X.; Ding, Y.; Liu, X.; Wu, Y.; Hayat, T.; Alsaedi, A.; Dai, S. Enhancing the Phase Stability of Inorganic α-$CsPbI_3$ by the Bication-Conjugated Organic Molecule for Efficient Perovskite Solar Cells. *ACS Applied Materials & Interfaces* **2019**, *11*, 37720–37725.

(11) Park, J.; Kim, J.; Yun, H.-S.; Paik, M. J.; Noh, E.; Mun, H. J.; Kim, M. G.; Shin, T. J.; Seok, S. I. Controlled growth of perovskite layers with volatile alkylammonium chlorides. *Nature* **2023**, *616*, 724–730.

(12) Wright, A. D.; Volonakis, G.; Borchert, J.; Davies, C. L.; Giustino, F.; Johnston, M. B.; Herz, L. M. Intrinsic quantum confinement in formamidinium lead triiodide perovskite. *Nat. Mater.* **2020**, *19*, 1201–1206.

(13) Elmestekawy, K. A.; Wright, A. D.; Lohmann, K. B.; Borchert, J.; Johnston, M. B.; Herz, L. M. Controlling Intrinsic Quantum Confinement in Formamidinium Lead Triiodide Perovskite through Cs Substitution. *ACS Nano* **2022**, *16*, 9640–9650.

(14) Utzat, H.; Sun, W.; Kaplan, A. E. K.; Krieg, F.; Ginterseder, M.; Spokoyny, B.; Klein, N. D.; Shulenberger, K. E.; Perkinson, C. F.; Kovalenko, M. V.; Bawendi, M. G. Coherent single-photon emission from colloidal lead halide perovskite quantum dots. *Science* **2019**, *363*, 1068–1072.

(15) Kaplan, A. E. K.; Krajewska, C. J.; Proppe, A. H.; Sun, W.; Sverko, T.; Berkinsky, D. B.; Utzat, H.; Bawendi, M. G. Hong–Ou–Mandel interference in colloidal CsPbBr3 perovskite nanocrystals. *Nat. Photon.* **2023**, *17*, 775–780.

(16) Chen, J.; Wang, J.; Xu, X.; Li, J.; Song, J.; Lan, S.; Liu, S.; Cai, B.; Han, B.; Precht, J. T.; Ginger, D.; Zeng, H. Efficient and bright white light-emitting diodes based on single-layer heterophase halide perovskites. *Nat. Photonics* **2021**, *15*, 238–244.

(17) Chen, J.; Xiang, H.; Wang, J.; Wang, R.; Li, Y.; Shan, Q.; Xu, X.; Dong, Y.; Wei, C.; Zeng, H. Perovskite White Light Emitting Diodes: Progress, Challenges, and Opportunities. *ACS Nano* **2021**, *15*, 17150–17174.

(18) Franchini, C.; Reticcioli, M.; Setvin, M.; Diebold, U. Polarons in materials. *Nature Reviews Materials* **2021**,

(19) Xing, G.; Mathews, N.; Sun, S.; Lim, S. S.; Lam, Y. M.; Grätzel, M.; Mhaisalkar, S.; Sum, T. C. Long-Range Balanced Electron- and Hole-Transport Lengths in Organic-Inorganic CH_3 NH_3 PbI_3. *Science* **2013**, *342*, 344–347.

(20) Cinquanta, E.; Meggiolaro, D.; Motti, S. G.; Gandini, M.; Alcocer, M. J.; Akkerman, Q. A.; Vozzi, C.; Manna, L.; De Angelis, F.; Petrozza, A.; Stagira, S. Ultrafast THz Probe of Photoinduced Polarons in Lead-Halide Perovskites. *Phys. Rev. Lett.* **2019**, *122*, 166601.

(21) Ghosh, D.; Welch, E.; , A. J.; Zakhidov, A.; Tretiak, S. Polarons in Halide Perovskites: A Perspective. *J. Phys. Chem. Lett.* **2020**, *11*, 3271–3286.

(22) Meggiolaro, D.; Ambrosio, F.; Mosconi, E.; Mahata, A.; De Angelis, F. Polarons in Metal Halide Perovskites. *Advanced Energy Materials* **2020**, *10*, 1902748.

(23) Baranowski, M.; Nowok, A.; Galkowski, K.; Dyksik, M.; Surrente, A.; Maude, D.; Zacharias, M.; Volonakis, G.; Stranks, S. D.; Even, J.; Maczka, M.; Nicholas, R.; Plochocka, P. Polaronic Mass Enhancement and Polaronic Excitons in Metal Halide Perovskites. *ACS Energy Lett.* **2024**, *9*, 2696–2702.

(24) Miyata, K.; Meggiolaro, D.; Trinh, M. T.; Joshi, P. P.; Mosconi, E.; Jones, S. C.; De Angelis, F.; Zhu, X.-Y. Large polarons in lead halide perovskites. *Sci. Adv.* **2017**, *3*, e1701217.

(25) Smith, M. D.; Jaffe, A.; Dohner, E. R.; Lindenberg, A. M.; Karunadasa, H. I. Structural origins of broadband emission from layered Pb–Br hybrid perovskites. *Chem. Sci.* **2017**, *8*, 4497–4504.

(26) Decrescent, R. A.; Du, X.; Kennard, R. M.; Venkatesan, N. R.; Dahlman, C. J.; Chabinyc, M. L.; Schuller, J. A. Even-Parity Self-Trapped Excitons Lead to Magnetic Dipole Radiation in Two-Dimensional Lead Halide Perovskites. *ACS Nano* **2020**, *14*, 8958–8968, Publisher: American Chemical Society.

(27) Han, Y.; Yin, J.; Cao, G.; Yin, Z.; Dong, Y.; Chen, R.; Zhang, Y.; Li, N.; Jin, S.; Mohammed, O. F.; Cui, B.-B.; Chen, Q. Exciton Self-Trapping for White Emission

in 100-Oriented Two-Dimensional Perovskites via Halogen Substitution. *ACS Energy Lett.* **2022**, *7*, 453–460.

(28) Tao, W.; Zhang, C.; Zhou, Q.; Zhao, Y.; Zhu, H. Momentarily trapped exciton polaron in two-dimensional lead halide perovskites. *Nat Commun* **2021**, *12*, 1400.

(29) Fu, J.; Ramesh, S.; Melvin Lim, J. W.; Sum, T. C. Carriers, Quasi-particles, and Collective Excitations in Halide Perovskites. *Chem. Rev.* **2023**, *123*, 8154–8231.

(30) Straus, D. B.; Guo, S.; Cava, R. J. Kinetically Stable Single Crystals of Perovskite-Phase CsPbI3. *Journal of the American Chemical Society* **2019**, *141*, 11435–11439.

(31) Buizza, L. R. V.; Herz, L. M. Polarons and Charge Localization in Metal-Halide Semiconductors for Photovoltaic and Light-Emitting Devices. *Advanced Materials* **2021**, *33*, 2007057.

(32) Rashba, E. I. Progress in exciton spectroscopy: personal perspective. *Journal of Luminescence* **2000**, *87-89*, 1–6.

(33) Sumi, H.; Sumi, A. Dimensionality Dependence in Self-Trapping of Excitons. *Journal of the Physical Society of Japan* **1994**, *63*, 637–657.

(34) Toyozawa, Y.; Shinozuka, Y. Stability of an Electron in Deformable Lattice: Force Range, Dimensionality and Potential Barrier. *Journal of the Physical Society of Japan* **1980**, *48*, 472–478.

(35) Woo, Y. W.; Li, Z.; Jung, Y.-K.; Park, J.-S.; Walsh, A. Inhomogeneous Defect Distribution in Mixed-Polytype Metal Halide Perovskites. *ACS Energy Lett.* **2023**, *8*, 356–360.

(36) Schilcher, M. J.; Robinson, P. J.; Abramovitch, D. J.; Tan, L. Z.; Rappe, A. M.; Reichman, D. R.; Egger, D. A. The Significance of Polarons and Dynamic Disorder in Halide Perovskites. *ACS Energy Letters* **2021**, 2162–2173.

(37) Ouhbi, H.; Wiktor, J. Polaron formation and hopping in tantalate perovskite oxides: NaTaO 3 and KTaO 3. *Phys. Rev. B* **2021**, *104*, 235158.

(38) Janotti, A.; Varley, J. B.; Choi, M.; Van de Walle, C. G. Vacancies and small polarons in SrTiO 3. *Phys. Rev. B* **2014**, *90*, 085202.

(39) Spreafico, C.; VandeVondele, J. The nature of excess electrons in anatase and rutile from hybrid DFT and RPA. *Phys. Chem. Chem. Phys.* **2014**, *16*, 26144–26152.

(40) Dabo, I.; Ferretti, A.; Poilvert, N.; Li, Y.; Marzari, N.; Cococcioni, M. Koopmans' condition for density-functional theory. *Phys. Rev. B* **2010**, *82*, 115121.

(41) Perdew, J. P.; Ernzerhof, M.; Burke, K. Rationale for mixing exact exchange with density functional approximations. *The Journal of Chemical Physics* **1996**, *105*, 9982–9985.

(42) Adamo, C.; Barone, V. Toward reliable density functional methods without adjustable parameters: The PBE0 model. *The Journal of Chemical Physics* **1999**, *110*, 6158–6170.

(43) Freysoldt, C.; Neugebauer, J.; Van de Walle, C. G. Fully Ab Initio Finite-Size Corrections for Charged-Defect Supercell Calculations. *Phys. Rev. Lett.* **2009**, *102*, 016402.

(44) Falletta, S.; Wiktor, J.; Pasquarello, A. Finite-size corrections of defect energy levels involving ionic polarization. *Physical Review B* **2020**, *102*, 041115.

(45) Kumagai, Y.; Oba, F. Electrostatics-based finite-size corrections for first-principles point defect calculations. *Phys. Rev. B* **2014**, *89*, 195205.

(46) Bischoff, T.; Wiktor, J.; Chen, W.; Pasquarello, A. Nonempirical hybrid functionals for band gaps of inorganic metal-halide perovskites. *Phys. Rev. Materials* **2019**, *3*, 123802.

(47) Huang, Y.; Yin, W.-J.; He, Y. Intrinsic Point Defects in Inorganic Cesium Lead Iodide Perovskite CsPbI $_3$. *J. Phys. Chem. C* **2018**, *122*, 1345–1350.

(48) Valastro, S.; Mannino, G.; Smecca, E.; Sanzaro, S.; Deretzis, I.; Magna, A. L.; Jena, A. K.; Miyasaka, T.; Alberti, A. Optical behaviour of γ-black $CsPbI_3$ phases formed by quenching from 80 °C and 325 °C. *J. Phys. Mater.* **2021**, *4*, 034011.

(49) Pham, T. D.; Deskins, N. A. Efficient Method for Modeling Polarons Using Electronic Structure Methods. *Journal of Chemical Theory and Computation* **2020**, *16*, 5264–5278.

(50) Mosquera-Lois, I.; Kavanagh, S. R.; Walsh, A.; Scanlon, D. O. ShakeNBreak: Navigating the defect configurational landscape. *Journal of Open Source Software* **2022**, *7*, 4817.

(51) Mosquera-Lois, I.; Kavanagh, S. R.; Walsh, A.; Scanlon, D. O. Identifying the ground state structures of point defects in solids. *npj Comput Mater* **2023**, *9*, 1–11, Number: 1 Publisher: Nature Publishing Group.

(52) Liu, Y.; Monserrat, B.; Wiktor, J. Strong electron-phonon coupling and bipolarons in Sb_2S_3. *Phys. Rev. Mater.* **2023**, *7*, 085401.

(53) Neukirch, A. J.; Nie, W.; Blancon, J.-C.; Appavoo, K.; Tsai, H.; Sfeir, M. Y.; Katan, C.; Pedesseau, L.; Even, J.; Crochet, J. J.; Gupta, G.; Mohite, A. D.; Tretiak, S. Polaron Stabilization by Cooperative Lattice Distortion and Cation Rotations in Hybrid Perovskite Materials. *Nano Lett.* **2016**, *16*, 3809–3816.

(54) Kresse, G.; Furthmüller, J. Efficient iterative schemes for ab initio total-energy calculations using a plane-wave basis set. *Physical Review B - Condensed Matter and Materials Physics* **1996**, *54*, 11169–11186.

(55) Kresse, G.; Furthmuller, J. Efficiency of ab-initio total energy calculations for metals and semiconductors using a plane-wave basis set. *Computational Materials Science* **1996**, *6*, 15–50.

(56) Blöchl, P. E. Projector augmented-wave method. *Phys. Rev. B* **1994**, *50*, 17953–17979.

(57) Monkhorst, H. J.; Pack, J. D. Special points for Brillouin-zone integrations. *Physical Review B* **1976**, *13*, 5188–5192.

(58) Perdew, J. P.; Ruzsinszky, A.; Csonka, G. I.; Vydrov, O. A.; Scuseria, G. E.; Constantin, L. A.; Zhou, X.; Burke, K. Restoring the Density-Gradient Expansion for Exchange in Solids and Surfaces. *Phys. Rev. Lett.* **2008**, *100*, 136406.

(59) Frost, J. M. Calculating polaron mobility in halide perovskites. *Physical Review B* **2017**, *96*.

(60) Ganose, A. M.; Park, J.; Faghaninia, A.; Woods-Robinson, R.; Persson, K. A.; Jain, A. Efficient calculation of carrier scattering rates from first principles. *Nature Communications* **2021**, *12*, 2222.

(61) Togo, A. First principles phonon calculations in materials science. *Scripta Materialia* **2015**, 5.

(62) Gonze, X.; Lee, C. Dynamical matrices, Born effective charges, dielectric permittivity tensors, and interatomic force constants from density-functional perturbation theory. *Phys. Rev. B* **1997**, *55*, 10355–10368.

(63) Chen, W.; Pasquarello, A. Correspondence of defect energy levels in hybrid density functional theory and many-body perturbation theory. *Physical Review B* **2013**, *88*, 115104.

(64) Freysoldt, C.; Grabowski, B.; Hickel, T.; Neugebauer, J.; Kresse, G.; Janotti, A.; Van De Walle, C. G. First-principles calculations for point defects in solids. *Reviews of Modern Physics* **2014**, *86*, 253–305.

(65) VandeVondele, J.; Krack, M.; Mohamed, F.; Parrinello, M.; Chassaing, T.; Hutter, J.

Quickstep: Fast and accurate density functional calculations using a mixed Gaussian and plane waves approach. *Computer Physics Communications* **2005**, *167*, 103–128.

(66) Kuhne, T. D. et al. CP2K: An electronic structure and molecular dynamics software package - Quickstep: Efficient and accurate electronic structure calculations. *The Journal of Chemical Physics* **2020**, *152*, 194103.

(67) VandeVondele, J.; Hutter, J. Gaussian basis sets for accurate calculations on molecular systems in gas and condensed phases. *The Journal of Chemical Physics* **2007**, *127*, 114105.

(68) Hartwigsen, C.; Goedecker, S.; Hutter, J. Relativistic separable dual-space Gaussian pseudopotentials from H to Rn. *Phys. Rev. B* **1998**, *58*, 3641–3662.

(69) Goedecker, S.; Teter, M.; Hutter, J. Separable dual-space Gaussian pseudopotentials. *Phys. Rev. B* **1996**, *54*, 1703–1710.

(70) Guidon, M.; Hutter, J.; VandeVondele, J. Auxiliary Density Matrix Methods for Hartree-Fock Exchange Calculations. *Journal of Chemical Theory and Computation* **2010**, *6*, 2348–2364.

(71) Nosé, S. A unified formulation of the constant temperature molecular dynamics methods. *The Journal of Chemical Physics* **1984**, *81*, 511–519.

(72) Hoover, W. G. Canonical dynamics: Equilibrium phase-space distributions. *Phys. Rev. A* **1985**, *31*, 1695–1697.

(73) Community, B. O. Blender - a 3D modelling and rendering package. Blender Foundation: Stichting Blender Foundation, Amsterdam, 2018.

(74) Wang, X.; Tian, T.; Aschauer, U. Beautiful Atoms: A python library for the manipulation and visualization of atomistic structure using blender. `https://github.com/beautiful-atoms/beautiful-atoms`.

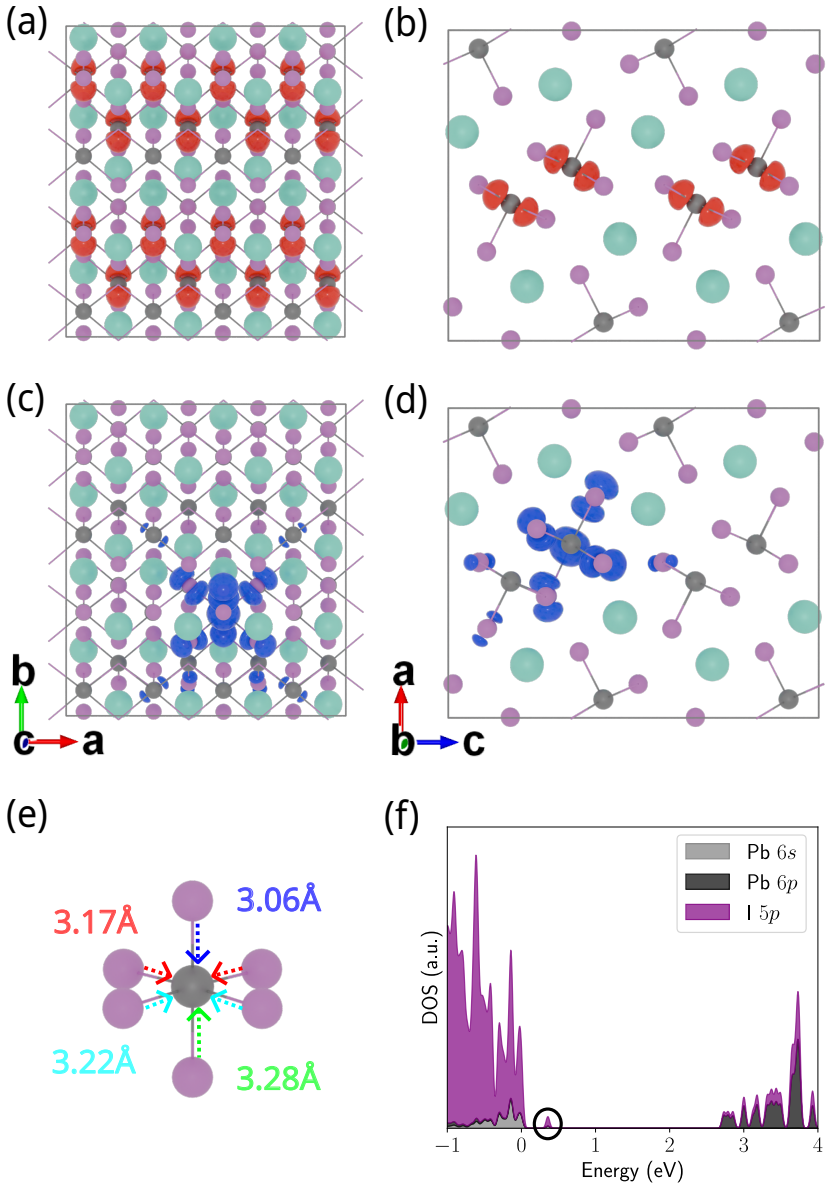

Figure 2: Polarons in δ-$CsPbI_3$. Wavefunction isosurface of the excess electron (a) and (b), and that of the hole polaron (c) and (d) as viewed from the c and b axes. (e) The Pb-I bond lengths of a [PbI_6] octahedron of the hole polaron with the arrows indicating the bond contractions. (f) PDOS of the relaxed hole polaronic structure, with the energetic location of the hole polaron circled.

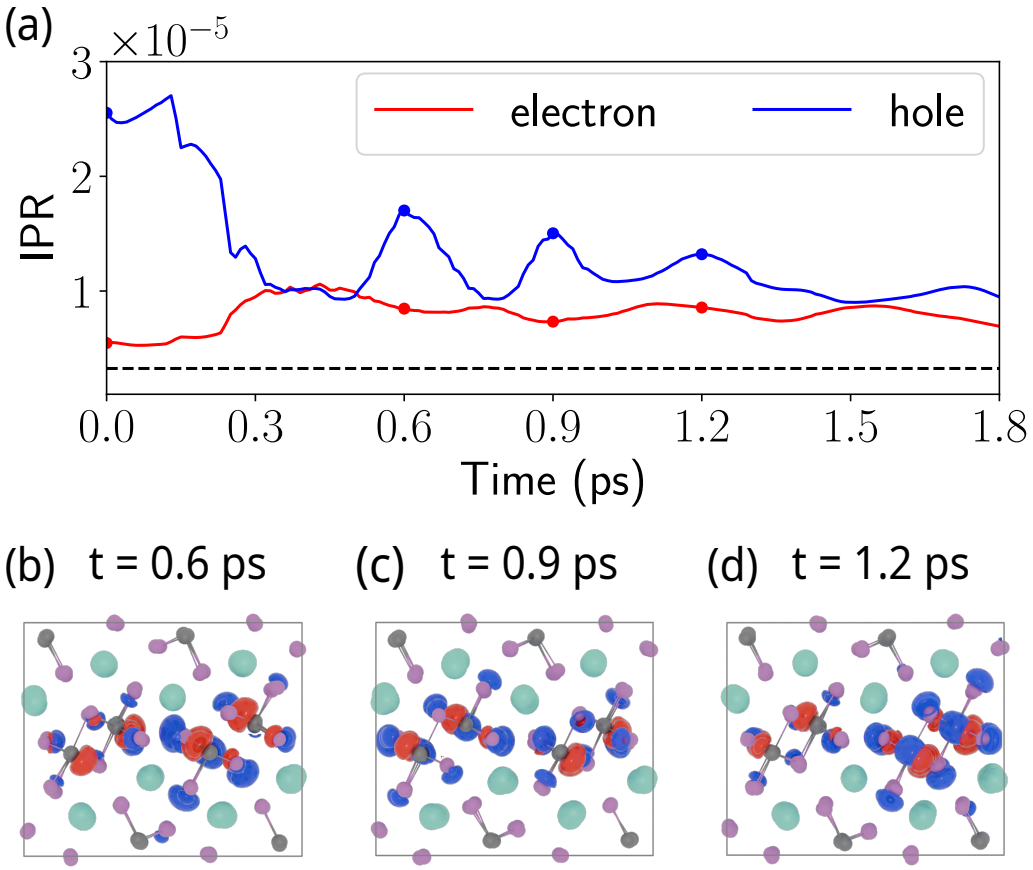

Figure 3: Molecular dynamics (MD) simulation with the electron and hole in the spin triplet configuration. (a) The inverse participation ratio (IPR) of the electron and hole wavefunction during the MD run. The dashed line represents the IPR value of a completely delocalized system. The electron and hole wavefunction isosurface at (b) $t = 0.6\,\mathrm{ps}$ (c) $t = 0.9\,\mathrm{ps}$ and (d) $t = 1.2\,\mathrm{ps}$.